Experimental Mechanics
DOI 10.1007/s11340-013-9717-6

Fast, Robust and Accurate Digital Image Correlation Calculation Without Redundant Computations

B. Pan · K. Li · W. Tong

Received: 22 October 2012 / Accepted: 8 January 2013

Abstract High-efficiency and high-accuracy deformation analysis using digital image correlation (DIC) has become increasingly important in recent years, considering the ongoing trend of using higher resolution digital cameras and common requirement of processing a large sequence of images recorded in a dynamic testing. In this work, to eliminate the redundant computations involved in conventional DIC method using forward additive matching strategy and classic Newton–Raphson (FA-NR) algorithm without sacrificing its sub-pixel registration accuracy, we proposed an equivalent but more efficient DIC method by combining inverse compositional matching strategy and Gauss-Newton (IC-GN) algorithm for fast, robust and accurate full-field displacement measurement. To this purpose, first, an efficient IC-GN algorithm, without the need of re-evaluating and inverting Hessian matrix in each iteration, is introduced to optimize the robust zero-mean normalized sum of squared difference (ZNSSD) criterion to determine the desired deformation parameters of each interrogated subset. Then, an improved reliability-guided displacement tracking strategy is employed to achieve further speed advantage by automatically providing accurate and complete initial guess of deformation for the IC-GN algorithm implemented on each calculation point. Finally, an easy-to-implement interpolation coefficient look-up table approach is employed to avoid the repeated calculation of bicubic interpolation at sub-pixel locations. With the above improvements, redundant calculations involved in various procedures (i.e. initial guess of deformation, sub-pixel displacement registration and sub-pixel intensity interpolation) of conventional DIC method are entirely eliminated. The registration accuracy and computational efficiency of the proposed DIC method are carefully tested using numerical experiments and real experimental images. Experimental results verify that the proposed DIC method using IC-GN algorithm and the existing DIC method using classic FA-NR algorithm generate similar results, but the former is about three to five times faster. The proposed reliability-guided IC-GN algorithm is expected to be a new standard full-field displacement tracking algorithm in DIC.

Keywords Digital image correlation · Image matching · Sub-pixel displacement · Inverse compositional image alignment algorithm · Newton–Raphson algorithm

B. Pan (✉)
Institute of Solid Mechanics, Beijing University of Aeronautics & Astronautics, Beijing 100191, China
e-mail: panb04@mails.tsinghua.edu.cn

K. Li
Department of Mechanical Engineering, Shanghai University, Shanghai 200444, China

W. Tong
Department of Mechanical Engineering, Southern Methodist University, Dallas, TX 75275, USA

Introduction

Digital image correlation (DIC) is a non-contact optical metrology for full-field motion, deformation and shape measurements. Since its invention in the early 1980s [1, 2], the method has undergone significant improvements in terms of registration accuracy, matching robustness, computational efficiency and application scope. It can be said that DIC is the most popular and widely used technique in the field of experimental mechanics [3–6]. In the practical implementation of DIC, reference square subsets centered at evenly spaced grids are specified in the reference image and used to track their

Published online: 07 February 2013

respective locations in the deformed images to retrieve full-field displacement vectors. Because it is common to track tens of thousands calculation points in a single image, the computational cost of DIC is generally considered to be very huge. With the ongoing trend of using higher resolution digital cameras, the number of points that need to be tracked in the recorded images keeps increasing. Moreover, considering the common requirement of processing a large sequence of digital images recorded in a dynamic testing and the special requirement of real-time motion tracking in certain applications, the computational efficiency of DIC method has become increasingly important in recent years [7–9].

In DIC, sub-pixel registration algorithm has been considered as a key technique to improve accuracy. It is interesting to find that most of the existing sub-pixel registration algorithms used in DIC employs an easy-to-understand forward additive matching strategy. Namely, the target subset deformed by an initial estimate of deformation is compared with the original square reference subset to solve for the incremental deformation parameters, which is subsequently added to the initial estimate to update the parameters. Accurate subset matching is normally completed through optimizing a non-linear correlation function using an iterative algorithm, for instance, the forward additive Newton–Raphson (FA-NR) algorithm originally proposed by Bruck HA et al. [10] and subsequently improved by others [11–16]. As a typical forward iterative DIC method, the FA-NR algorithm has now been commonly used for accurate sub-pixel displacement measurement [17], and recently it has also been refined to significantly improve its computational efficiency [9]. However, one inherent limitation of the FA-NR algorithm is that the Hessian matrix must be re-evaluated and inverted in every iteration. The calculation and inversion of Hessian matrix is a major computational burden of current forward iterative DIC method using classic FA-NR algorithm. Naturally, an equivalent but more efficient iterative sub-pixel registration algorithm without the need of re-evaluating and inverting Hessian matrix in each iteration is advantageous in improving the computational efficiency of the DIC method.

As a matter of fact, the forward additive matching algorithms are not the only way to calculate sub-pixel displacement [3, 18, 19]. It is noted that, in the field of computer vision, an efficient inverse compositional matching strategy combined with the Gauss-Newton (IC-GN) algorithm has been proposed by Baker and Matthews [20, 21] to align a template image to an input image. In Ref. [21], the IC-GN algorithm is provably equivalent to the classic forward additive image alignment algorithm, i.e. the famous Lucas-Kanade algorithm [22]. The latter is in essence a Gaussian-Newton algorithm, and is actually equivalent to the improved NR algorithm widely used in DIC in respect of basic principle and algorithm implementation [23]. Nevertheless, compared with Lucas-Kanade algorithm or FA-NR algorithm, the implementation of IC-GN algorithm is more efficient, as the Hessian matrix of IC-GN algorithm remains constant and can be pre-computed. The high efficiency of IC-GN algorithm motivates us to introduce it into DIC for fast and accurate full-field displacement measurement. However, the original IC-GN algorithm was implemented on a sum of squared difference (SSD) criterion, which is simple but less practical because any possible offset and/or scale changes in deformed image will lead to large errors in DIC measurements. In a practical measurement, deformed images may undergo certain amount of intensity changes [24, 25]. Thus, a robust and more practical correlation criterion should be used to accommodate the potential changes in illumination or ambient light. Besides, the original IC-GN algorithm was dedicated to simple template matching rather than full-field motion tracking. While implementing the IC-GN algorithm on a number of calculation points defined in a region of interest (ROI), the issue of how to offer an accurate initial guess for each measurement point should be carefully addressed, because just like the classic FA-NR algorithm, an inaccurate initial guess may cause IC-GN algorithm converge slowly or not at all. Due to this reason, the efficiency gain of IC-GN algorithm cannot be fully embodied without an accurate initial estimate of deformation. It is necessary to mention here that, in a recent book regarding DIC techniques written by Sutton MA et.al. [3], the IC-GN algorithm was used by the authors for full-field displacement measurement. However, they also fail to address the aforementioned issues regarding the more robust and efficient use of IC-GN algorithm.

The objective of this work is to develop a fast, robust and accurate DIC method, which adopts the more efficient IC-GN algorithm, instead of the classic FA-NR algorithm, for accurate full-field displacement measurement with sub-pixel accuracy. To make the best use of IC-GN algorithm, several innovations are made to the proposed DIC method to improve its robustness and computational efficiency. First, a robust and practical zero-mean normalized sum of square difference (ZNSSD) criterion, which allows for linear intensity variations of the target image, is employed to enhance the practicality of original IC-GN algorithm. Second, an improved reliability-guided displacement tracking initial guess transfer strategy adopting modified initial guess transfer scheme is used, which can not only intelligently guide the calculation path of DIC by avoiding error propagation, but also automatically provide very accurate initial estimate for the IC-GN algorithm implemented on each calculation point. Finally, an interpolation coefficient look-up table approach is used to avoid the redundant calculations involved in sub-pixel intensity interpolation. With these improvements, all redundant calculations involved in various procedures (i.e. initial guess of deformation, sub-pixel displacement registration and sub-pixel intensity interpolation) of conventional DIC calculation are entirely eliminated. The proposed DIC

method can achieve obvious speed advantages over existing FA-NR algorithm-based DIC method without sacrificing its accuracy. The accuracy and computational efficiency of the proposed DIC method are demonstrated by numerical and real experiments.

Inverse Compositional Gauss-Newton Algorithm for Accurate Sub-Pixel Registration

ZNSSD Criterion

The IC-GN algorithm was proposed by Baker and Matthews in 2001 [20] for efficient alignment of a template to a target image in computer vision. However, the original IC-GN algorithm was performed on a simple but less practical SSD criterion, which is sensitive to any potential intensity variations of the target image [24, 25]. In this work, the robustness of the original IC-GN algorithm is first improved by introducing a more practical and robust correlation criterion, which allows for linear intensity variations in the target image. Specifically, to quantitatively evaluate the similarity between the reference and target subsets, a practical and robust ZNSSD criterion, combined with an affine transform warping function, is used.

$$C_{\mathrm{ZNSSD}}(\Delta\mathbf{p}) = \sum_{\xi}\left\{\frac{[f(\mathbf{x}+\mathbf{W}(\boldsymbol{\xi};\Delta\mathbf{p}))-\overline{f}]}{\Delta f} - \frac{[g(\mathbf{x}+\mathbf{W}(\boldsymbol{\xi};\mathbf{p}))-\overline{g}]}{\Delta g}\right\}^2 \tag{1}$$

where f(**x**) and g(**x**) denote the grayscale levels at $x=(x, y, 1)^{\mathrm{T}}$ of reference image and the deformed image, and $\overline{f}=\frac{1}{N}\sum_{\xi} f(\mathbf{x}+\mathbf{W}(\boldsymbol{\xi};\Delta\mathbf{p}))$, $\overline{g}=\frac{1}{N}\sum_{\xi} g(\mathbf{x}+\mathbf{W}(\boldsymbol{\xi};\mathbf{p}))$ are the mean intensity value of the two subsets with N denotes the total number of points within the subset, $\Delta f=\sqrt{\left[\sum_{\xi} f(\mathbf{x}+\mathbf{W}(\boldsymbol{\xi};\Delta\mathbf{p}))-\overline{f}\right]^2}$ and $\Delta g=\sqrt{\left[\sum_{\xi} g(\mathbf{x}+\mathbf{W}(\boldsymbol{\xi};\mathbf{p}))-\overline{g}\right]^2}$. $\boldsymbol{\xi}=(\Delta x,\Delta y,1)^T$ is the local coordinates of the pixel point in each subset (Note that all image coordinates are expressed in a form of homogenous coordinate for notation brevity). **W**(ξ; **p**) is the warp function, also known as displacement mapping function in DIC, depicting the position and shape of the target subset relative to the reference subset; **W**(ξ; Δ**p**) is the incremental warp function exerted on the reference subset. We should note that $\overline{f}$ and Δf shown (equation (1)) are two statistical values of each reference subset. As they are irrelevant to the deformed image, these two values can be pre-computed for each reference subset. Efficient calculations of these two values can be accomplished using a global sum-table approach based on a fast recursive scheme [7].

It is worth noting that the ZNSSD correlation coefficient is actually related to the commonly used zero-mean normalized cross-correlation (ZNCC) criterion according to the equation of $C_{ZNCC}(\mathbf{p}) = 1 - 0.5 \times C_{ZNSSD}(\mathbf{p})$. Though the ZNCC coefficient falls into a range of [−1, 1] is more straightforward to show the similarity degree between the reference subset and target subset, the optimization of ZNSSD is much easier. Due to this reason, the ZNSSD criterion is optimized to determine the displacement components of each calculation point. Then, the ZNSSD coefficient is converted to the ZNCC coefficient according to their relations. In the following section, the optimized ZNCC coefficient of calculated points will be used as a reliability (or quality) index to ensure reliable and accurate initial guess transfer among consecutive calculation points.

Warp Function

In this work, a practical affine warp function (i.e. linear displacement mapping function) allowing rigid body translation, rotation, normal strain, shear strain and their combinations of the target subsets, is used.

$$W(\boldsymbol{\xi};\mathbf{p}) = \begin{bmatrix} 1+u_x & u_y & u \\ v_x & 1+v_y & v \\ 0 & 0 & 1 \end{bmatrix}\begin{pmatrix}\Delta x\\ \Delta y\\ 1\end{pmatrix} \tag{2}$$

where $p=(u, u_x, u_y, v, v_x, v_y)^{\boldsymbol{T}}$ is the pre-computed deformation parameter vector exerted on the target subset, with u, v denote the displacement components, and the other four parameters represent the displacement gradients of the considered subset.

To accurately match the two subsets, the roles of the target subset and reference subset are reversed in IC-GN algorithm. As schematically shown in Fig. 1, a backward matching strategy is used by exerting an incremental warping function **W**(ξ,Δ**p**) to the reference subset and comparing it with the target subset deformed by **W**(ξ,Δ**p**).

$$\mathbf{W}(\boldsymbol{\xi};\Delta\mathbf{p}) = \begin{bmatrix} \mathbf{1}+\Delta\mathbf{u_x} & \Delta\mathbf{u_y} & \Delta\mathbf{u} \\ \Delta\mathbf{v_x} & \mathbf{1}+\Delta\mathbf{v_y} & \Delta\mathbf{v} \\ \mathbf{0} & \mathbf{0} & \mathbf{1} \end{bmatrix}\begin{pmatrix}\Delta\mathbf{x}\\ \Delta\mathbf{y}\\ \mathbf{1}\end{pmatrix} \tag{3}$$

where $\Delta\mathbf{p} = \left(\Delta\mathbf{u}, \Delta\mathbf{u_x}, \Delta\mathbf{u_y}, \Delta\mathbf{v}, \Delta\mathbf{v_x}, \Delta\mathbf{v_y}\right)^{\mathbf{T}}$ denotes the incremental parameter vector to be determined.

The incremental warp can be solved by minimizing the similarity criterion given in (equation (1)). Subsequently, the incremental warp **W** (ξ; Δ**p**) is inverted and composed with the current estimate **W** (ξ; **p**) to get the updated warping function of the deformed subset [20]. In this sense, it is very different from the regular forward matching strategy currently used in DIC, where an incremental parameter vector Δ**p** is applied to the target subset deformed by **W** (ξ; **p**), and

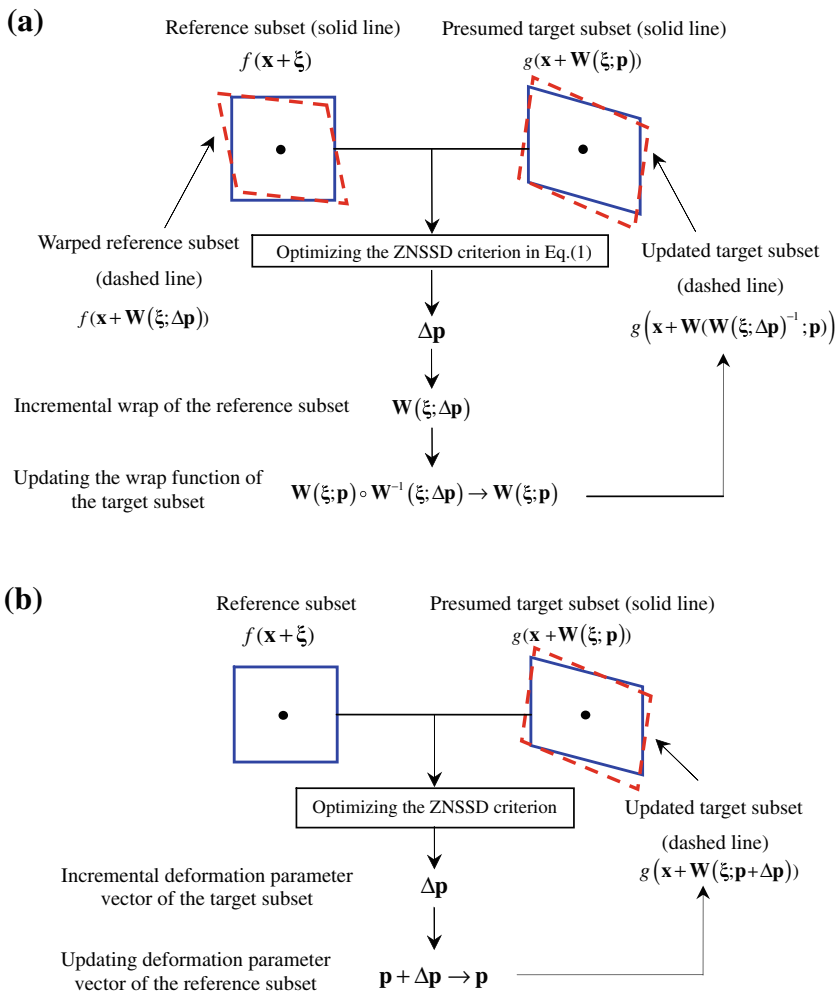

Fig. 1 Schematic drawing of: (**a**) the backward matching strategy of the IC-GN algorithm and (**b**) the forward matching strategy of the classic FA-NR algorithm

is then compared with the original reference subset to solve for $\Delta\mathbf{p}$, as schematically shown in Fig. 1(b).

Optimizing ZNSSD Criterion Using Gauss-Newton Algorithm

In order to solve for $\mathbf{W}(\xi;\Delta\mathbf{p})$, we first perform a first-order Taylor expansion of (equation (1)) with respect to $\Delta\mathbf{p}$. That yields

$$C_{\mathrm{ZNSSD}}(\Delta\mathbf{p}) = \sum_{\xi}\left[\frac{f(\mathbf{x}+\xi)+\nabla f\frac{\partial\mathbf{W}}{\partial\mathbf{p}}\Delta\mathbf{p}-\overline{\mathbf{f}}}{\Delta f}-\frac{g(\mathbf{x}+\mathbf{W}(\xi;\mathbf{p}))-\overline{g}}{\Delta g}\right]^2 \tag{4}$$

where $\nabla f=\left(\frac{\partial f(\mathbf{x}+\xi)}{\partial x},\frac{\partial f(\mathbf{x}+\xi)}{\partial y}\right)$ is the gradients of the reference subset. It is quite necessary to mention that the first-order derivatives of intensities f_x,f_y are calculated by convolving the gray matrix of the reference image with a mask of $[\frac{1}{12},-\frac{8}{12},0,\frac{8}{12},-\frac{1}{12}]$ in x, y direction respectively. The truncation error of this gradient operator is $o(h^4)$, much smaller than those of the sobel and prewitt gradient operators commonly used in digital image processing to extract the image border. $\frac{\partial\mathbf{W}}{\partial\mathbf{p}}=\begin{pmatrix}1&\Delta x&\Delta y&0&0&0\\0&0&0&1&\Delta x&\Delta y\end{pmatrix}$ is the Jacobian of the warp function. These two terms are constants and merely related to the reference image, so they can be pre-computed.

Minimization of the $C_{\mathrm{ZNSSD}}(\Delta\mathbf{p})$ with respect to $\Delta\mathbf{p}$, i.e. $\frac{\partial C_{\mathrm{ZNSSD}}(\Delta\mathbf{p})}{\partial(\Delta\mathbf{p})}=0$, gives the least-squares solution of $\Delta\mathbf{p}$.

$$\Delta\mathbf{p}=-\mathbf{H}_{6\times6}{}^{-1}\times\sum_{\xi}\left\{\left(\nabla\mathbf{f}\frac{\partial\mathbf{W}}{\partial\mathbf{p}}\right)^{\mathbf{T}}_{6\times1}\times\left[\left(\mathbf{f}(\mathbf{x}+\xi)-\overline{\mathbf{f}}\right)-\frac{\Delta\mathbf{f}}{\Delta\mathbf{g}}\left(\mathbf{g}(\mathbf{x}+\mathbf{W}(\xi;\mathbf{p}))-\overline{\mathbf{g}}\right)\right]\right\} \tag{5}$$

where H is the 6×6 Hessian Matrix given as

$$\mathbf{H}_{6\times6}=\sum_{\xi}\left[\left(\nabla f\frac{\partial \mathbf{W}}{\partial \mathbf{p}}\right)^{T}_{6\times1}\times\left(\nabla f\frac{\partial \mathbf{W}}{\partial \mathbf{p}}\right)_{1\times6}\right] \tag{6}$$

Equation (6) shows that the Hessian matrix relies only on the local gradients of reference subset $\nabla f(\mathrm{x}+\boldsymbol{\xi})$ and the Jacobian of the warp function $\frac{\partial \mathbf{W}}{\partial \mathbf{p}}$. It is clear that there is nothing in the Hessian matrix **H** that depends on **p**, so it is constant during iteration and can be pre-computed [20, 21]. In this way, the repeated calculation and inverse of Hessian matrix in classic FA-NR algorithm are eliminated. Besides, (equation (5)) shows merely the intensity at sub-pixel locations, i.e. $g(\mathbf{x}+\mathbf{W}(\boldsymbol{\xi};\mathbf{p}))$, must be provided for the implementation of IC-GN algorithm, whereas both the intensities and intensity gradients, say $g(\mathbf{x}+\mathbf{W}(\boldsymbol{\xi};\mathbf{p}))$, $g_x(\mathbf{x}+\mathbf{W}(\boldsymbol{\xi};\mathbf{p}))$, $g_y(\mathbf{x}+\mathbf{W}(\boldsymbol{\xi};\mathbf{p}))$, must be estimated for the classic FA-NR algorithm. In this respect, the IC-GN algorithm achieves further computational efficiency compared with FA-NR algorithm.

Updating Warp Function

Based on the obtained parameter vector $\Delta\mathbf{p}$, the incremental warp $\mathbf{W}(\boldsymbol{\xi};\Delta\mathbf{p})$ of the reference subset can be determined. Then, the incremental warp is inverted and composed with the current estimate $\mathbf{W}(\boldsymbol{\xi};\mathbf{p})$ to generate the updated warp function of the target subset.

$$\begin{aligned}\mathbf{W}(\boldsymbol{\xi};\mathbf{p}) &\leftarrow \mathbf{W}(\boldsymbol{\xi};\mathbf{p})\circ\mathbf{W}^{-1}(\boldsymbol{\xi};\Delta\mathbf{p})\\ &=\begin{bmatrix}1+\mathbf{u_x} & \mathbf{u_y} & \mathbf{u}\\ \mathbf{v_x} & 1+\mathbf{v_y} & \mathbf{v}\\ \mathbf{0} & \mathbf{0} & \mathbf{1}\end{bmatrix}\begin{bmatrix}1+\Delta\mathbf{u_x} & \Delta\mathbf{u_y} & \Delta\mathbf{u}\\ \Delta\mathbf{v_x} & 1+\Delta\mathbf{v_y} & \Delta\mathbf{v}\\ \mathbf{0} & \mathbf{0} & \mathbf{1}\end{bmatrix}^{-1}\end{aligned} \tag{7}$$

where $\mathbf{W}(\boldsymbol{\xi};\Delta\mathbf{p})^{-1}$ denotes the inverted incremental warp function.

Convergence Conditions

Equation (5) is repeated until a predefined convergence condition is satisfied. In this work, the convergence conditions are set to ensure that variations in the norm of the incremental deformation parameter is equal to or less than 0.001, i.e., $\|\Delta\mathbf{p}\|=\sqrt{(\Delta u)^2+(max(\Delta x)\times\Delta u_x)^2+(max(\Delta y)\times\Delta u_y)^2+(\Delta v)^2+(max(\Delta x)\times\Delta v_x)^2+(max(\Delta y)\times\Delta v_y)^2}\le 0.001$.

Efficient Implementation of IC-GN Algorithm Without Redundant Computations

Reliability-Guided Displacement Tracking Strategy Using Improved Initial Guess Transfer Scheme

In the above section, one evident shortcoming of the original IC-GN algorithm is overcame by introducing a more robust and practical ZNSSD criterion. However, as a common feature of all non-linear local optimization algorithms, the convergence characteristic of IC-GN algorithm relies heavily on the provided initial guess. In other words, an accurate initial guess, reasonably close to the true value, must be provided to ensure the algorithm to converge correctly and rapidly. Otherwise, the IC-GN algorithm may converge slowly or not converges at all. Regrettably, the IC-GN algorithm was originally developed for simple template matching rather than full-field motion tracking [20, 21]. Therefore, the issue of how to provide accurate initial guess in an efficient manner for the IC-GN algorithm to be performed at a number of pre-defined calculation points must be carefully addressed.

To make the best use of IC-GN algorithm for fast full-field displacement tracking, a simple but effective reliability-guided displacement tracking strategy [14, 15], capable of providing complete and very accurate initial guess for each calculation point, is used in conjunction with the IC-GN algorithm in this work. The detailed implementation procedure of the reliability-guided displacement tracking strategy is summarized as follows.

Step 1: Specify a seed point (or starting point) in the ROI defined in the reference image, whose initial guess can be accurately and reliably determined using various automatic searching schemes [5, 7, 26, 27] or manually in the deformed image [5]. Then, the six deformation parameters and the ZNCC coefficient of the single seed point are optimized using the aforementioned IC-GN algorithm. Afterwards, the correlated seed point is marked as a calculated point and inserted into a queue. Note that each calculated point is inserted into a position in the queue according to its matching quality, which can be quantified using ZNCC coefficient. That means all the points in the queue are ordered according to their ZNCC coefficient from the higher to lower, and the point with highest ZNCC coefficient is placed at the top of the queue.

Step 2: If the queue is not empty, remove the first point, which has the highest reliability (i.e. maximum ZNCC coefficient), from the top of the queue. Next, analyze each of its four neighboring points of interest. If it is a valid point and hasn't been computed, it will then be processed using the IC-GN method to obtain its six deformation parameters and ZNCC correlation coefficient. To provide an accurate initial guess for the neighboring calculation points and ensure a fast and correct convergence of the IC-GN algorithm, an improved initial guess transfer scheme considering the distance between the two points and local displacement gradients is

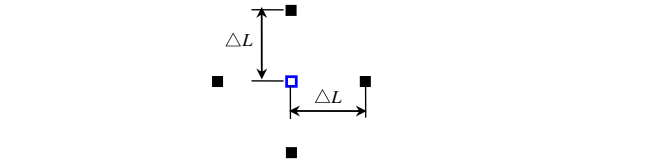

Fig. 2 Schematic drawing showing the improved initial guess transfer scheme considering the distance and displacement gradients between adjacent calculation points

adopted as schematically shown in Fig. 2. Specifically, the initial guess of the neighboring points, denoted by $\mathbf{p}_{\mathbf{NP}(\text{Neighboring point})} = \left(u^0_{\mathbf{NP}}, u^0_{x\_\mathbf{NP}}, u^0_{y\_\mathbf{NP}}, v^0_{\mathbf{NP}}, v^0_{x\_\mathbf{NP}}, v^0_{y\_\mathbf{NP}}\right)$, is computed from the computed deformation parameters of the removed point, denoted as $\mathbf{p}_{\mathbf{RP}(\text{removed point})} = \left(u_{\mathbf{RP}}, u_{x\_\mathbf{RP}}, u_{y\_\mathbf{RP}}, u_y, v_{\mathbf{RP}}, v_{x\_\mathbf{RP}}, v_{y\_\mathbf{RP}}\right)^T$, as follows.

$$\begin{aligned} u^0_{\mathbf{NP}} &= u_{\mathbf{RP}} + u_{x\_\mathbf{RP}} \times \Delta L + u_{y\_\mathbf{RP}} \times \Delta L \\ u^0_{x\_\mathbf{NP}} &= u_{x\_\mathbf{RP}} \\ u^0_{y\_\mathbf{NP}} &= u_{y\_\mathbf{RP}} \\ v^0_{\mathbf{NP}} &= v_{\mathbf{RP}} + v_{x\_\mathbf{RP}} \times \Delta L + v_{y\_\mathbf{RP}} \times \Delta L \\ v^0_{x\_\mathbf{NP}} &= v_{x\_\mathbf{RP}} \\ v^0_{y\_\mathbf{NP}} &= v_{y\_\mathbf{RP}} \end{aligned} \tag{8}$$

where ΔL is pre-defined grid step, i.e. the distance between two adjacent calculation points. We should note that, compared with the directly initial guess transfer scheme used previously [8, 14, 15], the initial guess obtained by (equation (8)) will provide more accurate initial guess by taking the local displacement gradients into consideration [27, 28]. When the deformed images involve large relative deformation and/or rotation or a large grid step is used, initial guess estimated by (equation (8)) is more accurate. As a consequence, the IC-GN algorithm will exhibit better convergence characteristics with less average iteration number, indicating higher computational efficiency.

Then, each of the just calculated points is labeled and inserted into the queue according to its ZNCC coefficient value.

Step 3: Repeat step 2 until the queue is empty, which means that all the valid points in the ROI have been computed and the image correlation computation is completed.

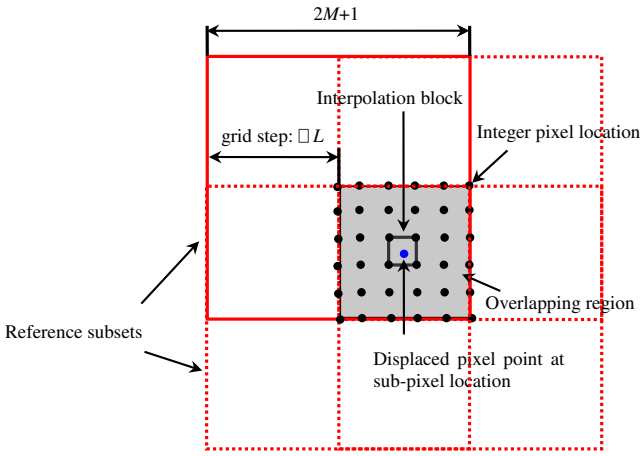

Fig. 3 Schematic diagram showing redundant interpolation involved in conventional FA-NR algorithm: the displaced pixel point (*blue dot*) repeatedly appears at adjacent subsets (*dashed line*) as the reference subsets defined in reference image overlap each other, which means redundant interpolation calculations during the optimization of various subsets

From the above description, it is clear that the calculation path of IC-GN algorithm is automatically guided by the ZNCC coefficient of computed points, rather than a simple pointwise scanning strategy along each column or row. The reliability-guided displacement tracking strategy guarantees that the neighbors of the point with highest reliability (indicated by its ZNCC coefficient) will be processed first. The improved initial guess transfer scheme of (equation (8)) ensures that more accurate deformation parameters are automatically transferred to current calculation point.

The merits of reliability-guided displacement tracking strategy are embodied in the following three aspects: 1) **Accurateness**: a complete initial guess more close to true value can be estimated using (equation (8)), and an accurate initial guess helps to speed the convergence of the IC-GN algorithm implemented later; 2) **Efficiency**: conventional initial guess approach based on a simple but time-consuming integer-pixel displacement searching is entirely avoided; 3) **Robustness**: the reliability-guided displacement tracking strategy can intelligently guide the calculation path of DIC, and is therefore generally applicable to specimens with irregular shape and/or subject to discontinuous deformation [14, 15, 29].

Interpolation Coefficient Look-up Table for Bicubic Interpolation

Also, (equation (5)) shows that, during the implementation of IC-GN algorithm, the intensity at subpixel positions, i.e. g ($\mathbf{x}$+$\mathbf{W}$ ($\boldsymbol{\xi}$; $\mathbf{p}$)), located among neighboring four integer pixels, must be reconstructed using certain subpixel interpolation scheme. The selection of interpolation scheme is a key factor that affects the calculation accuracy

and convergence character of IACA algorithm. In this work, the generalized bicubic interpolation scheme [30, 31] is implemented to determine the gray values at sub-pixel locations as follows:

$$g(x,y) = \sum_{m=0}^{3}\sum_{n=0}^{3} \alpha_{mn} x^m y^n \tag{9}$$

where the unknown 16 coefficients, i.e., a_{00}, a_{01}, …, a_{33}, of (equation (9)) can be determined by the gray intensity of the neighboring 4×4 pixels centered at the sub-pixel location.

It is natural to carry out sup-pixel interpolation for each sub-pixel position when necessary. However, this seemingly straightforward approach is very time-consuming, because the iterative algorithm normally repeats more than one time before its convergence, which means that each pixel with the considered subset should be interpolated repeatedly for several times. Also, due to the high overlap between adjacent subsets, the pixel point within one reference subset may also appear in its neighboring reference subsets as shown in Fig. 3, which means that further repetitive interpolation must be performed on the same pixel point. Considering the following example, if a subset of $(2M+1)\times(2M+1)$ pixels and a grid step of ΔL pixels are chosen for DIC calculation, each pixel within the considered subset will also be used in its adjacent $\left[\text{floor}\left(\frac{2M+1}{\Delta L}\right)+1\right]^2$ reference subsets, where floor(x) denotes the largest integer less than x. Suppose the IC-GN algorithm needs an average iteration number of n_{ave} times to average, it is therefore estimated that the 16 interpolation coefficients required in (equation (9)) will be repeatedly calculated $n_{ave} \times \left[\text{floor}\left(\frac{2M+1}{\Delta L}\right)+1\right]^2$ times. More specifically, for a moderate subset of 41×41 pixels subset, a grid step of 5 pixels and an ordinary average iteration of 3 times, the bicubic interpolation will be repeated for about 243 times for each pixel within an interrogated subset.

It is worth mentioning that the 16 coefficients remain the same for each interpolation block, regardless of the specific sub-pixel locations within it. This fact enlightens us to develop an interpolation coefficient look-up table approach to eliminate the redundant calculations involved in the sub-pixel intensity reconstruction. The interpolation coefficient look-up table approach builds a two-dimensional empty matrix (i.e., lookup table) with the same size of the digital image, with each element in the matrix denoting the interpolation coefficients of each interpolation block. For each sub-pixel position where sub-pixel intensity interpolation is required, the algorithm first judges the corresponding position in the look-up table. If it is empty, the bicubic interpolation will be carried out, and subsequently the 16 interpolation coefficients of the particular interpolation block are saved in the lookup table. Otherwise, the already computed 16 interpolation coefficients are directly used to avoid repeated estimation of bicubic interpolation coefficients. In this way, for the same example given above, the bicubic interpolation needs to be implemented merely once, rather than 243 times, for each interpolation block.

Experimental Verification

Verification the Accuracy and Precision of IC-GN Algorithm Using Numerical Tests

To quantitatively compare the calculation accuracy and precision of the proposed DIC method using IC-GN algorithm with the regular DIC method using FA-NR algorithm, numerical experiments are utilized in this study. Figure 4 shows the speckle pattern used in the following numerical experiments. The 8-bit speckle pattern with a resolution of 768×576 pixels was taken from our previous experiment. In the following numerical studies only pure in-plane translation tests were performed. A series of translated speckle images for each speckle pattern were generated by applying the appropriate shift in Fourier domain according to shift theorem [32]. The sub-pixel displacements applied in x direction range from 0 to 1 pixel, corresponding to a shift of 0.05 pixels between two successive images. Moreover, to simulate the image noise, additive random Gaussian noise with a mean value of 0 and a variance of 4, was added to each image to simulate the influence of noise. The displacements of each translated speckle pattern were computed at regularly distributed 2,501(=61×41) points (the distance between neighboring points is 10 pixels) using both the proposed DIC method described above and the conventional DIC method introduced in detail in Ref. [8]. Note that both DIC codes were written in C++ language, and all the calculations were performed on a desk computer (4 cores of Inter (R) Core (TM) i5 CPU 750 with 2.67 GHz main frequency).

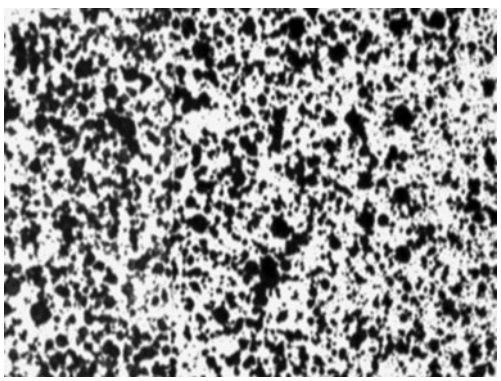

Fig. 4 Speckle pattern used in numerical experiment

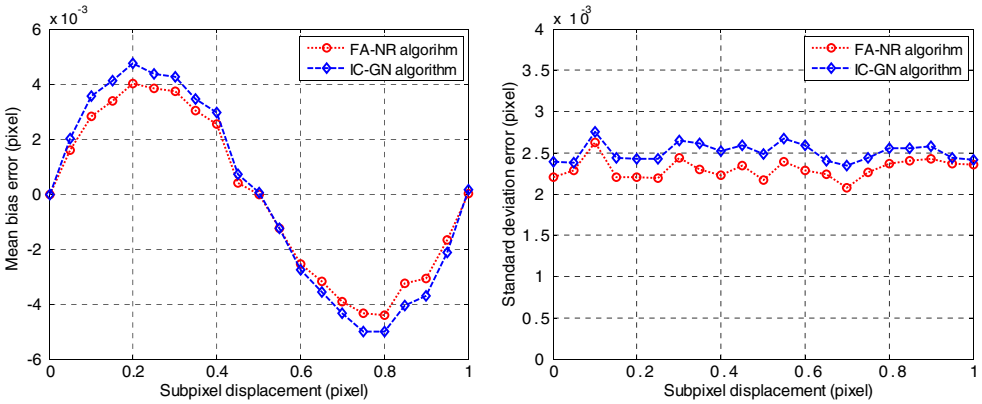

Fig. 5 Mean bias errors (*left*) and standard deviation errors (*right*) of measured *u*-displacement as a function of sub-pixel displacement for the proposed IC-GN algorithm and FA-NR algorithm using 31×31 pixels subset

To quantitatively evaluate the calculated displacements of the two different DIC methods and compare them with the imposed ones, the errors of the computed displacements are decomposed into two components: mean bias error (or systematic error) and standard deviation error (or random error). The mean bias error of the measured displacement is defined as:

$$u_e = u_{mean} - u_{imp} \tag{10}$$

where $u_{mean} = \frac{1}{N}\sum_{i=1}^{N} u_i$ represents the mean of the N estimated displacements and u_{imp} denotes the actual imposed sub-pixel displacement.

The standard deviation error of the measured displacement can be defined as:

$$\sigma_u = \sqrt{\frac{1}{N-1}\sum_{i=1}^{N}\left(u_{mean} - u_{imp}\right)^2} \tag{11}$$

The standard deviation error reflects the deviation of the measured displacement corresponding to the mean value.

Figure 5 shows the mean bias errors and standard deviation errors of displacements detected by the two difference DIC algorithms as a function of applied sub-pixel displacements using a 31×31 pixels subset. Note that the mean bias error of DIC is a function of subpixel displacement, which is approximately sinusoidal distribution with a period of 1 pixel. This kind of systematic error distribution can be attributed to positional intensity interpolation error on sub-pixel reconstruction [32, 33]. In contrast, the standard deviation errors of DIC are approximately stable and do not depend on the imposed sub-pixel displacement, which is more dependent of the quality of the speckle pattern and the subset size used for calculation [32]. From Fig. 5, it is seen that both the two DIC methods generate very similar results. The negligible differences can be attributed to the different algorithm implementation of the two algorithms. The experimental results verify the equivalence of the two DIC methods.

Verification the Robustness of IC-GN Algorithm Using Numerical Tests

To validate the robustness of the IC-GN algorithm using ZNSSD criterion over the existing IC-GN algorithm using SSD criterion [21], computer simulated speckle patterns were used. First, a reference speckle pattern comprising of 1,200 speckle granules, each speckle with a radius of 4 pixels, was generated first according to the simulation algorithm in Ref. [17]. Then, a uniaxial tensile strain of u_x= 0.005 (other deformation parameters being 0) was applied to the reference speckle pattern to generate a deformed speckle image. To simulate illumination intensity variations, the intensity of the deformed image was artificially adjusted with 20 % increase in brightness and 20 % decrease in contrast. Figure 6 shows the reference speckle image, the strained speckle image and the final speckle image with artificially changed brightness and contrast.

The strained speckle image (u_x=0.005) were processed with the IC-GN algorithm using ZNSSD criterion and conventional IC-GN algorithm using SSD criterion. In the analysis, the displacements were calculated with a subset of 31× 31 pixels and a distance of 5 pixels between consecutive calculation points. The calculation region is shown in the left image of Fig. 6. The analysis results of the *u*-field displacements using two different criteria are shown in Fig. 7. It is observed that the calculations of the conventional SSD criterion are seriously affected by the intensity

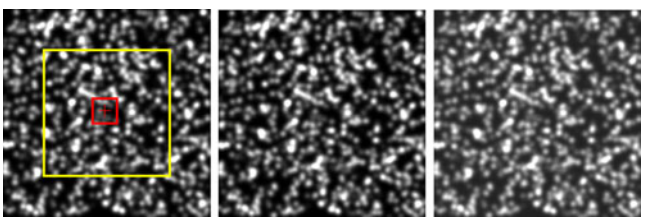

Fig. 6 Reference image (*left*), deformed image (*middle*), deformed image after artificially adjusted with 20 % increase in brightness and 20 % decreases in contrast (*right*). The yellow rectangular of the reference image indicates the specified region of interest and the red square is the subset used for calculation

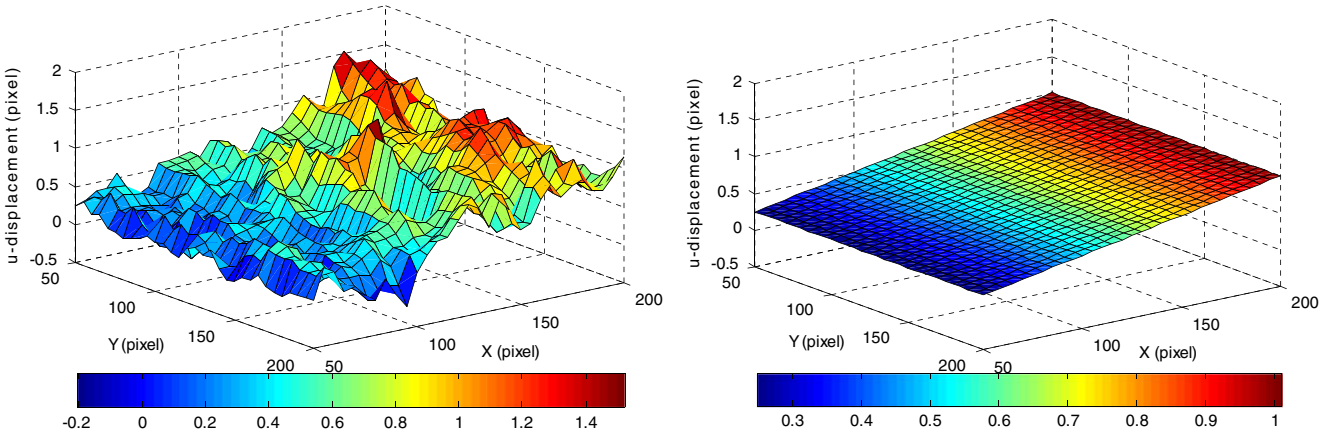

Fig. 7 Calculated u-field displacements (in units of pixel) for the uniaxially strained speckle patterns using the IC-GN algorithm with (**a**) a SSD criterion, (**b**) a ZNSSD criterion

changes in the deformed image. On the contrary, the ZNSSD criterion copes very well with the intensity variations, and it provides accurate measurement results that are in very good accordance with the theoretical ones. Because real experimental images may undergo variations in exposure and/or lighting during loading, the IC-GN algorithm using practical ZNSSD criterion is more robust.

Verification the Computational Efficiency of IC-GN Algorithm Using Real Experimental Images

To further verify the computational efficiency of the proposed DIC method, a real three-point-bending experiment was performed on a rubber specimen. Reference image and deformed image with a size of 1,280×1,024 pixels at 8-bit gray levels were taken without loading and after a loading of 300 N, as shown in Fig. 8 (a) and (b). A rectangular region of interest (ROI) containing 4,212 (=36×117) regularly spaced points were processed using the proposed DIC method based on IC-GN algorithm and the conventional DIC method using FA-NR algorithm we recently reported in Ref. [9].

Figure 9(a) and (b) show the *x*-directional, *y*-directional displacement fields computed by the proposed DIC method using a 41×41 pixels subset at a gird step of 10 pixels. In Fig. 9 (a), the neutral surface and anti-symmetric *u*-displacement of the bended rubber beam can be clearly discerned as expected, confirming the correctness of the measured displacements. It is also seen from Fig. 9(c) that the ZNCC coefficient of most calculated points are larger than 0.96 with an average ZNCC value of 0.979. The high ZNCC coefficients further verify the correctness of the calculated results. Although not shown here, we should note that the classic FA-NR algorithm produces almost identical results. A quantitative comparison between two computations shows that the absolute maximum differences in the *u*-displacement, *v*-displacement and ZNCC correlation coefficient are 0.0155 pixels, 0.0150 pixels and 0.0003, respectively. These minor differences may be caused by the different calculation scheme used and are acceptable in most calculations.

Figure 10 compares the computational efficiency of the proposed DIC and the recently proposed fast FA-NR algorithm at different subset sizes with a fixed grid step of 10 pixels. In this case, totally 4,212 points were analyzed. Compared with the fast FA-NR algorithm, the proposed DIC method increase the computational speed by approximately three to five times, the gain in computational efficiency is mainly attributed to: 1) the elimination of repeated calculation and inversion of Hessian matrix through the use of IC-GN algorithm; 2) the elimination of reconstruction of intensity gradients at sub-pixel locations in IC-GN algorithm; 3) the better convergence characteristics gained in IC-GN algorithm through implementing the improved initial

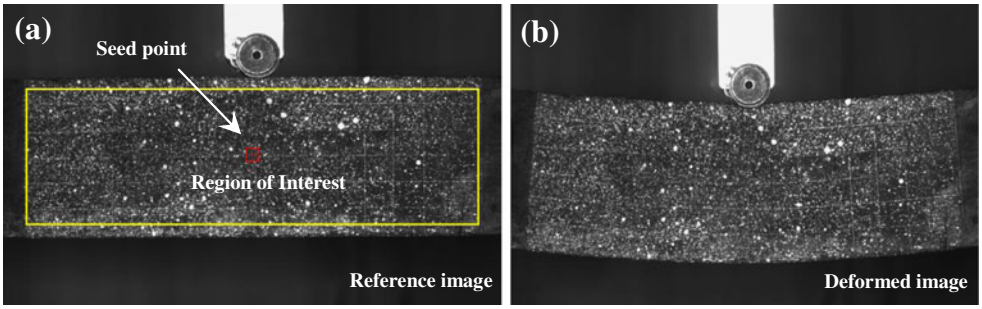

Fig. 8 Real experimental images of a rubber specimen subjected to three-point bending: (**a**) reference image and (**b**) deformed image

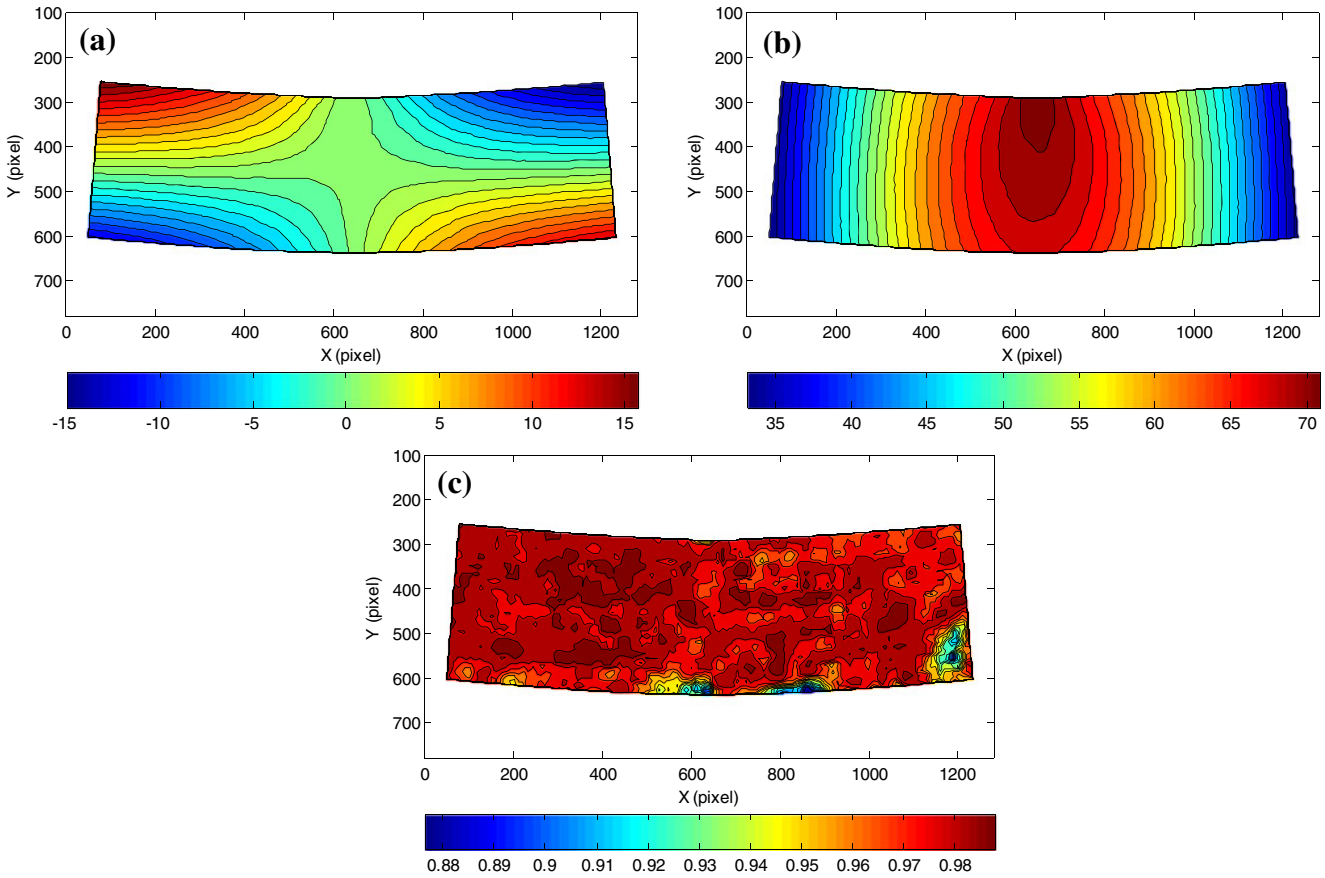

Fig. 9 Calculation of the rubber specimen using the proposed IC-GN algorithm-based DIC method with a subset of 41×41 pixels: (**a**) u-displacement field, (**b**) v-displacement field and (**c**) ZNCC coefficient distributions

guess transfer scheme. We also should note that the results indicated in Fig. 10 and Table 1 only show relative computational efficiency of one algorithm *versus* the other, and not an absolute computational speed, which depends on a number of factors, such as the converge conditions, use of programming language, programming efficiency as well as the performance of hardware.

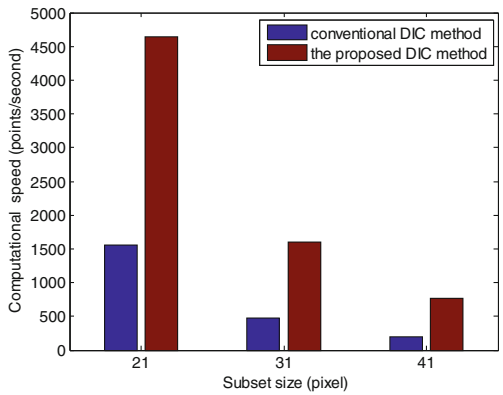

Fig. 10 A comparison of the computational speed of the proposed DIC algorithm and conventional DIC method using various subset sizes. The inserted table displays the computational speed and average iteration number in detail

Table 1 compares the average iterations and computational speeds of the IC-GN algorithm using various initial guess transfer scheme at different grid step, ranging from 5 pixels to 20 pixels, for a fixed subset size of 41×41 pixels. As shown, the average iteration of the direct initial guess transfer scheme increases with gird step. When the grid step increases from 5 pixels to 20 pixels, the average iterations of IC-GN algorithm using direct initial guess transfer scheme increase from 3.6 to 5.1 times, and the computational speed reduces correspondingly from 552 points/s to 383 points/s. This clearly proves the accurateness of initial guess estimated

Table 1 Comparison of the average iteration and the computational speed of IC-GN algorithm using direct initial guess transfer scheme and the improved initial guess transfer scheme at various grid step

Grid step (pixels)	Average iteration/calculation speed (p/s)	
	Direct initial guess transfer scheme	Improved initial guess transfer scheme
5	3.6/552	2.4/1701
10	4.1/482	2.6/1627
20	5.1/383	2.8/1564

by direct initial guess transfer scheme is lessened when a large grid step is used. By comparison, the average iterations of IC-GN algorithm using the improved initial guess transfer scheme remains virtually the same at different grid step. The decrease in average iteration and the increase in calculation speed prove that the improved initial guess transfer scheme using (equation (8)) provides more accurate initial guess for IC-GN algorithm, resulting in a faster convergence and higher computational speed of IC-GN algorithm.

Figure 11 quantitatively compares the prediction errors (i.e., the differences between the initial guesses of the displacement components and the final optimized displacement components) of the two initial guess transfer schemes for the two experimental images shown in Fig. 8. Note the DIC calculation was implemented using a subset size of 41×41 pixels and a grid step of 10 pixels. Figure 11 (a) shows the prediction errors in u-displacement (left) and v-displacement (right) using the direct initial guess transfer scheme. The prediction errors are within a wide range of [−0.8 0.8] pixels, and the root mean square errors are estimated to be 0.4126 pixels for u-displacement and 0.4697 pixels for v-displacement, respectively. By contrast, Fig. 11 (b) shows the prediction errors in u-displacement (left) and v-displacement using the improved initial guess transfer scheme. It is clear that, by taking the local strains into consideration, the improved initial guess transfer scheme provides more accurate initial guess of deformation. The prediction errors locate in a narrower range of [−0.2 0.3] pixels, and the corresponding RMS errors are merely 0.0222 pixels for u-displacement, and 0.0250 pixels for v-displacement, being one order of magnitude smaller than those of the former initial guess scheme.

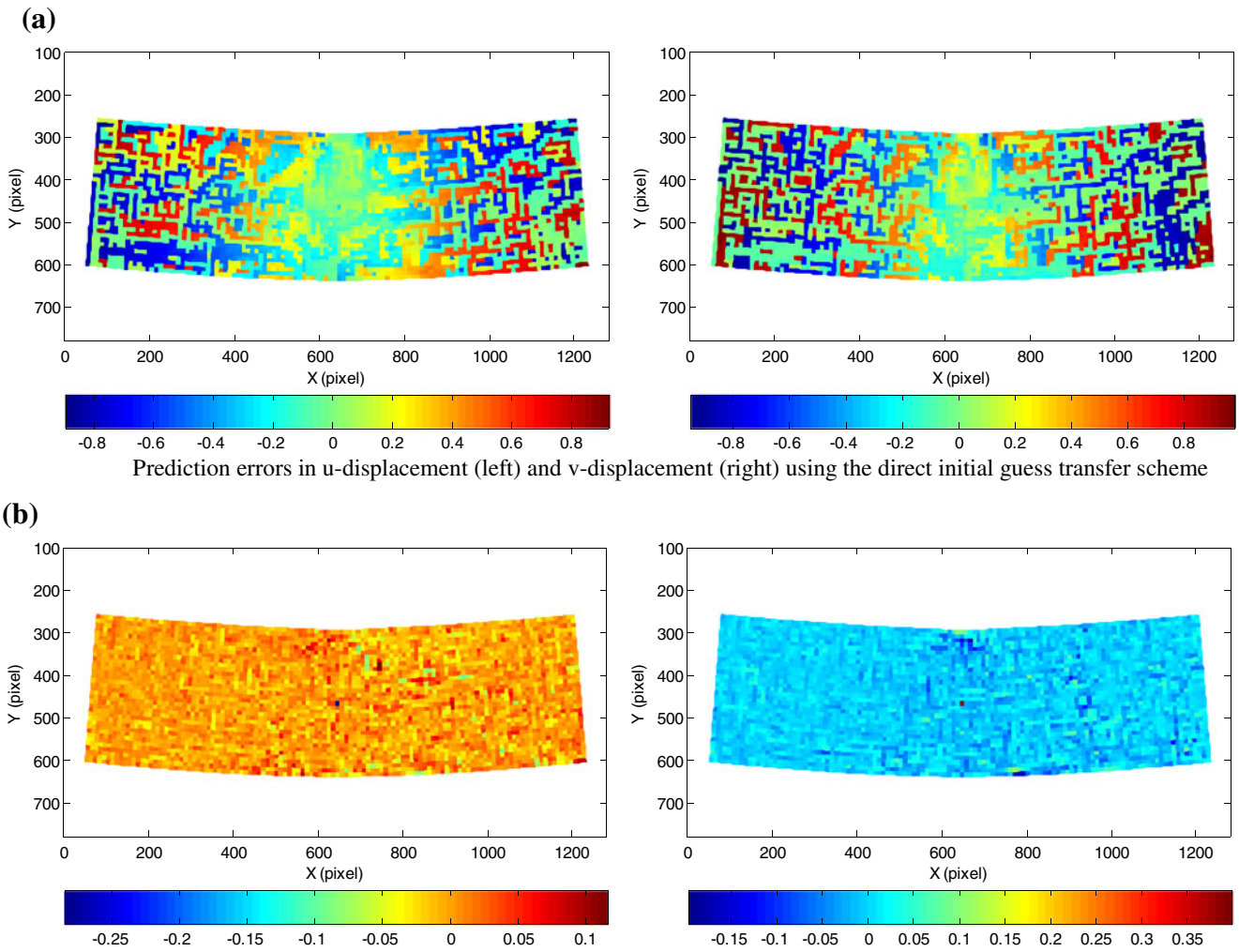

Fig. 11 Comparison of the prediction errors of the direct initial guess transfer scheme and the improved initial guess transfer scheme. (**a**) Prediction errors in u-displacement (*left*) and v-displacement (*right*) using the direct initial guess transfer scheme. (**b**) Prediction errors in u-displacement (*left*) and v-displacement (*right*) using the improved initial guess transfer scheme

Conclusion

Digital image correlation method using forward iterative matching strategy, typically the classic FA-NR algorithm, have been widely used and commonly accepted for deformation analysis. In this paper, we propose an equivalent but more efficient DIC method for full-field deformation analysis. The developed DIC method combines an efficient IC-GN algorithm using the practical ZNSSD correlation criterion, an improved reliability-guided displacement tracking strategy using modified initial guess transfer scheme and an elegant interpolation coefficient look-up table approach. With these innovations, all the redundant calculations involved in various stages of DIC calculation, i.e. initial guess of deformation vector, subpixel displacement registration and sub-pixel intensity interpolation calculation are entirely eliminated. Experimental results show that the proposed IC-GN-algorithm-based DIC method generates similar results as the classic FA-NR-algorithm-based DIC method does, but it is about three to five times faster dependent on the particular calculation settings. As an efficient, robust and accuracy algorithm for full-field displacement measurement, the proposed reliability-guided IC-GN-algorithm is expected to be a standard displacement tracking algorithm in DIC and should have more applications in various time-critical problems.

Acknowledgments This work reported here is supported by the National Natural Science Foundation of China (Grant Nos. 11272032, 11002012 and 91216301), the Program for New Century Excellent Talents in University, the China Aerospace Science and Technology Innovation Fund Project (Grant No. CASC201101), the Aeronautical Science Foundation of China (Grant No. 2011ZD51043), the Specialized Research Fund for the Doctoral Program of Higher Education (Grant No. 20101102120015).

References

1. Peters WH, Ranson WF (1981) Digital imaging techniques in experimental stress analysis. Opt Eng 21:427–431
2. Chu TC, Ranson WF, Sutton MA, Peters WH (1985) Applications of digital-image-correlation techniques to experimental mechanics. Exp Mech 25:232–244
3. Sutton MA, Orteu JJ, Schreier HW (2009) Image correlation for shape, motion and deformation measurements. Springer
4. Pan B, Qian KM, Xie HM, Asundi A (2009) Two-dimensional digital image correlation for in-plane displacement and strain measurement: a review. Meas Sci Technol 20:062001
5. Pan B (2011) Recent progress in digital image correlation. Exp Mech 51:1223–1235
6. Hild F, Roux S (2006) Digital image correlation: from displacement measurement to identification of elastic properties—a review. Strain 42(2):69–80
7. Huang JY, Zhu T, Pan XY, Qin L, Peng XL, Xiong CY, Fang J (2010) A high-efficiency digital image correlation method based on a fast recursive scheme. Meas Sci Technol 21:035101
8. Wang ZY, Hoang TM, Nguyen DA, Urcinas AC, Magro JR (2010) High-speed digital-image correlation method: comment. Opt Lett 35:2891
9. Pan B, Li K (2011) A fast digital image correlation method for deformation measurement. Opt Lasers Eng 49:841–847
10. Bruck HA, McNeil SR, Sutton MA, Peters WH (1989) Digital image correlation using Newton–Raphson method of partial differential correction. Exp Mech 29:261–267
11. Vendroux G, Knauss WG (1998) Submicron deformation field measurements: Part 2. Improved digital image correlation. Exp Mech 38:86–92
12. Lu H, Cary PD (2000) Deformation measurement by digital image correlation: implementation of a second-order displacement gradient. Exp Mech 40:393–400
13. Pan B, Xie HM, Guo ZQ, Hua T (2007) Full-field strain measurement using a two-dimensional Savitzky-Golay digital differentiator in digital image correlation. Opt Eng 46(3):033601
14. Pan B (2009) Reliability-guided digital image correlation for image deformation measurement. Appl Opt 48:1535–1542
15. Pan B, Wang ZY, Lu ZX (2010) Genuine full-field deformation measurement of an object with complex shape using reliability-guided digital image correlation. Opt Express 18:1011–1023
16. Huang J, Pan X, Peng X, Yuan Y, Xiong C, Fang J, Yuan F (2012) Digital image correlation with self-adaptive Gaussian windows. Exp Mech, 10.1007/s11340-012-9639-8
17. Pan B, Xie HM, Xu BQ, Dai FL (2006) Performance of sub-pixel registration algorithms in digital image correlation. Meas Sci Tech 17(6):1615–1621
18. Tong W, Yao H, Xuan Y (2011) An improved error evaluation in one-dimensional deformation measurements by linear digital image correlation. Exp Mech 51(9):1019–1031
19. Tong W (2011) Subpixel image registration with reduced bias. Opt Lett 36(5):763–765
20. Baker S, Mattews I (2001) Equivalence and efficiency of image alignment algorithms. Proc IEEE Conf Comput Vis Pattern Recognit 56:1090–1097
21. Baker S, Mattews I (2004) Lucas-Kanade 20 years on: a unifying framework. Int J Comput Vision 56:221–255
22. Lucas B, Kanade T (1981) An iterative image registration technique with an application to stereo vision. In Proceedings of the International Joint Conference on Artificial Intelligence, 674–679
23. Pan B, Asundi A, Xie HM, Gao JX (2009) Digital image correlation using iterative least squares and pointwise least squares for displacement field and strain field measurements. Opt Lasers Eng 47(7–8):865–874
24. Tong W (2005) An evaluation of digital image correlation criteria for strain mapping applications. Strain 41(4):167–175
25. Pan B, Xie HM, Wang ZY (2010) Equivalence of digital image correlation criteria for pattern matching. Appl Opt 49:5501–5509
26. Zhang JQ, Zeng P, Lei LP, Ma Y (2012) Initial guess by improved population-based intelligent algorithms for large inter-frame deformation measurement using digital image correlation. Opt Lasers Eng 50(3):473–490
27. Zhou YH, Pan B, Chen YQ (2012) Large deformation measurement using digital image correlation: a full automatic approach. Appl Opt 51(31):7674–7683
28. Zhou YH, Chen YQ (2012) Propagation function for accurate initialization and efficiency enhancement of digital image correlation. Opt Lasers Eng 50(12):1789–1797

29. Pan B, Wu DF, Xia Y (2010) High-temperature deformation field measurement by combing transient aerodynamic heating system and reliability-guided digital image correlation. Opt Lasers Eng 48 (9):841–848
30. Press WH (2003) C++ numerical algorithms. Publishing House of Electronics Industry, Beijing
31. http://en.wikipedia.org/wiki/Bicubic_interpolation
32. Pan B, Lu ZX, Xie HM (2010) Mean intensity gradient: an effective global parameter for quality assessment of the speckle patterns used in digital image correlation. Opt Lasers Eng 48(4):469–477
33. Wang YQ, Sutton MA, Bruch HA, Schreier HW (2009) Quantitative error assessment in pattern matching: effects of intensity pattern noise, interpolation, strain and image contrast on motion measurement. Strain 45:160–178